

# Lawrence Berkeley National Laboratory

## Lawrence Berkeley National Laboratory

### Title

A method for quick assessment of CO<sub>2</sub> storage capacity in closed and semi-closed saline formations

### Permalink

<https://escholarship.org/uc/item/0zh3x61x>

### Authors

Zhou, Q.  
Birkholzer, J.  
Tsang, C.F.  
[et al.](#)

### Publication Date

2008-06-25

1       **A Method for Quick Assessment of CO<sub>2</sub> Storage Capacity in Closed and**  
2                                   **Semi-Closed Saline Formations**

3  
4  
5  
6           Quanlin Zhou\*, Jens T. Birkholzer, Chin-Fu Tsang, and Jonny Rutqvist

7  
8                   Earth Sciences Division, Lawrence Berkeley National Laboratory,

9  
10                           University of California, Berkeley, CA 94720, USA  
11  
12

13                   \*Corresponding Author, Tel: 1-510-486-5748, Fax: 1-510-486-5686; Email:  
14                           [qzhou@lbl.gov](mailto:qzhou@lbl.gov), Mail Address: One Cyclotron Road, MS 90-1116

15 **Abstract:** Saline aquifers of high permeability bounded by overlying/underlying seals  
16 may be surrounded laterally by low-permeability zones, possibly caused by natural  
17 heterogeneity and/or faulting. Carbon dioxide (CO<sub>2</sub>) injection into and storage in such  
18 “closed” systems with impervious seals, or “semi-closed” systems with nonideal (low-  
19 permeability) seals, is different from that in “open” systems, from which the displaced  
20 brine can easily escape laterally. In closed or semi-closed systems, the pressure buildup  
21 caused by continuous industrial-scale CO<sub>2</sub> injection may have a limiting effect on CO<sub>2</sub>  
22 storage capacity, because geomechanical damage caused by overpressure needs to be  
23 avoided. In this research, a simple analytical method was developed for the quick  
24 assessment of the CO<sub>2</sub> storage capacity in such closed and semi-closed systems. This  
25 quick-assessment method is based on the fact that native brine (of an equivalent volume)  
26 displaced by the cumulative injected CO<sub>2</sub> occupies additional pore volume within the  
27 storage formation and the seals, provided by pore and brine compressibility in response to  
28 pressure buildup. With nonideal seals, brine may also leak through the seals into  
29 overlying/underlying formations. The quick-assessment method calculates these brine  
30 displacement contributions in response to an estimated average pressure buildup in the  
31 storage reservoir. The CO<sub>2</sub> storage capacity and the transient domain-averaged pressure  
32 buildup estimated through the quick-assessment method were compared with the “true”  
33 values obtained using detailed numerical simulations of CO<sub>2</sub> and brine transport in a two-  
34 dimensional radial system. The good agreement indicates that the proposed method can  
35 produce reasonable approximations for storage-formation-seal systems of various  
36 geometric and hydrogeological properties.

37 **Keywords:** geological CO<sub>2</sub> sequestration; storage capacity; saline aquifer; pressure  
38 buildup; numerical simulation

## 39 **1. Introduction**

40 Geological carbon dioxide (CO<sub>2</sub>) sequestration in deep formations (e.g., saline aquifers,  
41 gas and oil reservoirs, and coal beds) is a promising measure for mitigating the impact of  
42 climate change (Bachu et al., 1994, 2002; Koide et al., 1992; IPCC, 2005; van der Meer,  
43 1992). Reliable estimates are needed for the CO<sub>2</sub> storage capacity of geologic basins  
44 (Bradshaw et al., 2007). Currently, basin-scale storage capacity is often estimated based  
45 on the effective pore volume of suitable formations (i.e., those formations with sufficient  
46 injectivity, size, and long-term CO<sub>2</sub> containment capability). The effectiveness, or the  
47 storage efficiency factor, of suitable formations describes the fraction of total pore space  
48 available for CO<sub>2</sub> storage, limited by heterogeneity, buoyancy effects, residual water  
49 saturation, etc. (Bachu and Adams, 2003). Guidelines for estimating the storage capacity  
50 of deep saline formations were recently developed by the Capacity and Fairways  
51 Subgroup of the Geological Working Group of the U.S. Department of Energy (USDOE)  
52 Carbon Sequestration Regional Partnerships (USDOE, 2007). The current practice  
53 generally involves estimating storage capacity of “open” formations (Figure 1, top), from  
54 which the native fluid can easily escape laterally and make room for the injected CO<sub>2</sub>  
55 (e.g., Doughty and Pruess, 2004; Holloway et al., 1996; Shafeen et al., 2004; van der  
56 Meer, 1995). For such open formations, the pressure buildup caused by CO<sub>2</sub> injection is  
57 usually not a limiting factor except for maximum bottom-hole pressure at the injection  
58 well. However, the large amount of native brine laterally displaced by injected CO<sub>2</sub> in  
59 open systems may have a hydrological and geochemical impact on shallow groundwater

60 resources (Birkholzer et al., 2007; Nicot, 2008), an issue not addressed directly in this  
61 paper.

62 In certain geological situations, a storage basin may be composed of a number of  
63 compartmentalized reservoirs laterally separated by low-permeability zones. These zones  
64 may be formed by natural heterogeneity and/or faulting. When such a reservoir, bounded  
65 vertically by impervious seals, is surrounded on all sides by barriers of very low  
66 permeability, this reservoir acts as a “closed” system (Figure 1, middle) (i.e., there is  
67 negligible hydraulic communication with other formations during the injection period of  
68 interest, usually 30–50 years). Evidence of such closed systems has been found in  
69 hydrocarbon reservoirs, as indicated by sharp changes in fluid pressure along their  
70 boundaries (Muggeridge et al., 2004; Neuzil, 1995; Puckette and Al-Shaieb, 2003).  
71 Examples of such closed systems also include natural CO<sub>2</sub> reservoirs of high purity,  
72 which can be used as analogues for geological CO<sub>2</sub> sequestration (e.g., Allis et al., 2001;  
73 Pearce et al., 1996; Stevens et al., 2001). When large volumes of CO<sub>2</sub> are injected into a  
74 compartmentalized formation, which acts like a closed system (with the time scale of  
75 interest being the CO<sub>2</sub> injection period), a significant pressure buildup will be produced  
76 (e.g., Holloway et al., 1996; Polak et al., 2004). This pressure buildup can severely limit  
77 the CO<sub>2</sub> storage capacity, because overpressure-associated geomechanical damage needs  
78 to be avoided (Rutqvist and Tsang, 2002; Rutqvist et al., 2007). In this case, the storage  
79 capacity mainly depends on pore and brine compressibilities that provide expanded pore  
80 space available for storing the injected CO<sub>2</sub>, and on the maximum pressure buildup that  
81 the formation can sustain.

82 Of course, the overlying and underlying seals of a storage aquifer are not perfectly  
83 impervious, allowing the pressure buildup caused by CO<sub>2</sub> injection and storage to  
84 partially dissipate into and through these seals. In this case, the saline aquifer acts like a  
85 “semi-closed” system (Figure 1, bottom), allowing some fraction of the displaced brine to  
86 migrate into and through the overlying and underlying sealing units, which in turn would  
87 increase the storage capacity for CO<sub>2</sub>. (Meanwhile, the stored CO<sub>2</sub> is safely contained  
88 within the storage formation because of permeability and capillary barriers.) The  
89 importance of this vertical interlayer communication mostly depends on the permeability  
90 of the seals, which can vary widely (from 10<sup>-23</sup> to 10<sup>-16</sup> m<sup>2</sup>, or from 10<sup>-8</sup> to 10<sup>-1</sup> mD)  
91 depending on their hydrogeological characteristics (e.g., Domenico and Schwartz, 1998;  
92 Hart et al., 2006; Hovorka et al., 2001; Neuzil, 1994). Relatively permeable sealing units  
93 (e.g., with permeability on the order of 10<sup>-18</sup> m<sup>2</sup> or higher) may allow considerable  
94 vertical brine leakage out of the storage reservoir over the injection period. In this case,  
95 the pressure buildup may be reduced, and pressure constraints may not be a limiting  
96 factor in CO<sub>2</sub> storage.

97 Our research aims at developing a method for the quick assessment of CO<sub>2</sub> storage  
98 capacity in deep closed and semi-closed saline formations, complementing existing  
99 methods for capacity estimates in open systems (USDOE, 2007). This method can be  
100 used to estimate the storage efficiency factor and the transient domain-averaged pressure  
101 buildup. The validity of the method is demonstrated by comparing the estimated storage  
102 capacities to the “true” values calculated through detailed modeling of multiphase flow  
103 and multicomponent transport of CO<sub>2</sub> and brine. The modeling was conducted using the  
104 TOUGH2/ECO2N code, which has been tested and compared with other codes (Pruess,

105 2005; Pruess et al., 2004). The validity range is demonstrated for a range of hypothetical  
106 formation-seal systems, with varying lateral radial extent (i.e., pore volume) and  
107 hydrogeological properties (i.e., permeability and pore compressibility) of the storage  
108 formation and sealing units.

## 109 **2. A Quick-Assessment Method for CO<sub>2</sub> Storage Capacity**

110 We developed a simple method for assessing the storage capacity of closed and semi-  
111 closed storage formations. The basic principle is that CO<sub>2</sub> injection into these systems  
112 will lead to pressurization (pressure buildup), because an additional volume of fluid  
113 needs to be stored. The injected CO<sub>2</sub> displaces an equivalent volume of native brine,  
114 which may either (1) be stored in the expanded pore space in the storage formation, (2)  
115 be stored in the expanded pore space in the seals, or (3) leak through the seals into  
116 overlying/underlying formations. The quick-assessment method predicts the pressure-  
117 buildup history over a given injection period and the “actual” storage efficiency factor at  
118 the end of injection. We define the storage efficiency factor,  $E$ , as the volumetric fraction  
119 of stored CO<sub>2</sub>, per unit initial total pore volume of the storage formation, similar to the  
120 earlier definition for open systems (USDOE, 2007). The method is designed to provide  
121 capacity estimates at early stages of site selection and characterization, when (1) quick  
122 assessments of multiple sites may be needed and when (2) site characterization data are  
123 rather sparse. More specifically, the estimated pressure increase caused by injection and  
124 storage of a specified volume of CO<sub>2</sub> can be compared to a sustainable pressure  
125 threshold, which is the maximum pressure that the formation can sustain without  
126 geomechanical damage. Alternatively, one may determine the maximum CO<sub>2</sub> volume

127 that can be injected without jeopardizing the geomechanical structure of the formation-  
128 seal system.

## 129 **2.1. Simplifications and Assumptions**

130 Several simplifications and assumptions of both reservoir characteristics (geometric and  
131 hydrogeological properties) and processes made in the quick-assessment method are  
132 outlined below for an idealized, two-dimensional radial formation-seal system:

- 133 • The homogeneous storage formation for CO<sub>2</sub> sequestration is of radial extent  $R$  and  
134 thickness  $B_f$ , with an initial porosity  $\phi_f$ . The initial total pore volume is  
135  $V_f = \phi_f AB_f = \pi R^2 \phi_f B_f$ , where  $A$  is the horizontal area. The storage formation has a  
136 pore compressibility  $\beta_p$  ( $= \frac{1}{\phi_f} \frac{\partial \phi'_f}{\partial p}$ , where  $\phi'_f$  is the storage formation porosity,  
137 dependent on pressure change), which includes the possible contribution of vertical  
138 formation expansion and reflects the confining pressure and overburden stress prior to  
139 CO<sub>2</sub> injection.
- 140 • The upper and lower homogeneous seals have a uniform, identical thickness,  $B_s$ ,  
141 permeability  $k_s$ , porosity  $\phi_s$ , and pore compressibility  $\beta_{ps}$ . The total pore volume of  
142 both seals is  $V_s = 2\phi_s AB_s$ .
- 143 • The native brine has compressibility,  $\beta_w$  ( $= \frac{1}{\rho_w} \frac{\partial \rho_w}{\partial p}$ ), representing the change in  
144 brine density ( $\rho_w$ ) in response to pressure buildup, and viscosity,  $\mu_w$ , dependent on  
145 temperature, pressure, and salinity at the initial time of injection.
- 146 • The above hydrogeological parameters are assumed to be constant over the relevant  
147 range of pressure conditions, from the initial hydrostatic pressure to the elevated  
148 pressure value under final storage conditions. Only porosity changes are considered in  
149 response to pressure increases.
- 150 • The storage formation has uniform pressure buildup at any time of injection,  
151 independent of formation permeability. This overpressure decreases linearly through  
152 the seals to the hydrostatic pressure (prior to CO<sub>2</sub> injection) assumed at the top of the  
153 overlying seal and at the bottom of the underlying seal.



154 • All injected CO<sub>2</sub> mass is contained as a CO<sub>2</sub>-rich phase, with negligible dissolved  
 155 CO<sub>2</sub> mass within the storage formation. The total volume of stored CO<sub>2</sub> depends on  
 156 CO<sub>2</sub> density, which in turn depends on temperature and transient pressure conditions.  
 157 • Native brine leakage occurs through the entire formation-seal interface with a  
 158 uniform leakage rate, independent of CO<sub>2</sub> plume extent.  
 159 The validity of some of these assumptions is discussed in Section 4, based on the detailed  
 160 simulation results presented in Section 3. Note that the storage formation can have any  
 161 shape with varying thickness, because only its total pore volume is used in the quick-  
 162 assessment method. Specifications on the geometry of the storage formation have been  
 163 chosen for easier comparison with numerical simulation results.

## 164 2.2. Basic Equations

165 The quick-assessment method considers that the pore volume needed to store injected  
 166 CO<sub>2</sub>,  $V_{CO_2}(t_I)$ , after a given injection time,  $t_I$ , is provided by three contributions: (1) the  
 167 expanded storage volume in the storage formation resulting from pressure buildup, (2)  
 168 the expanded storage volume within the seals resulting from pressure buildup, and (3) the  
 169 volumetric leakage of brine into the formations above the upper seal and below the lower  
 170 seal. The expanded storage volume is caused by both brine and pore compressibility. A  
 171 simple expression describes this volumetric relationship, as follows:

$$172 \quad V_{CO_2}(t_I) = (\beta_p + \beta_w) \Delta p(t_I) V_f + 0.5 (\beta_{ps} + \beta_w) \Delta p(t_I) V_s + \int_0^{t_I} \frac{2Ak_s \Delta p(t)}{\mu_w B_s} dt, \quad (1)$$

173 where  $\Delta p(t_I)$  is the pressure buildup at time  $t_I$ ,  $\Delta p(t)$  ( $t = [0, t_I]$ ) is the transient  
 174 pressure buildup from the beginning to the end of injection, and the factor of 0.5 stems  
 175 from the assumption of linear pressure buildup from zero at the top of the overlying seal  
 176 (and the bottom of the underlying seal) to the storage-formation value at the formation-

177 seal interfaces. Each of the three terms on the right-hand side of Equation (1) corresponds  
 178 to one of the three storage contributions mentioned above. Equation (1) essentially links  
 179  $V_{CO_2}(t_I)$  to the average pressure buildup in the storage formation. By solving Equation  
 180 (1) for  $t_I$ , the total pressure buildup in the closed or semi-closed formation can be  
 181 assessed as a function of  $V_{CO_2}(t_I)$ .

182 Based on the definition of the storage efficiency factor and Equation (1), the storage  
 183 efficiency factor,  $E(t_I)$ , for a semi-closed system can be calculated:

$$184 \quad E(t_I) = (\beta_p + \beta_w)\Delta p(t_I) + 0.5(\beta_{ps} + \beta_w)\frac{V_s}{V_f}\Delta p(t_I) + \int_0^{t_I} \frac{2Ak_s\Delta p(t)}{\mu_w B_s V_f} dt, \quad (2)$$

185 where the storage efficiency factor consists of three individual efficiency contributions  
 186 from expanded pore volume in the storage formation and the seals, as well as from brine  
 187 leakage into the underlying and overlying formations. To compare the relative  
 188 importance of the three individual contributions, we define the volumetric fractions of  
 189 displaced brine stored in the storage formation ( $F_f$ ), in the seals ( $F_s$ ), and in the  
 190 overlying/underlying formations ( $F_l$ ), relative to the total pore volume storing CO<sub>2</sub>, as  
 191 follows:

$$192 \quad F_f = (\beta_p + \beta_w)\Delta p(t_I)V_f/V_{CO_2}(t_I), \quad (3a)$$

$$193 \quad F_s = 0.5(\beta_{ps} + \beta_w)\Delta p(t_I)V_s/V_{CO_2}(t_I), \quad (3b)$$

$$194 \quad F_l = \int_0^{t_I} \frac{2Ak_s\Delta p(t)}{\mu_w B_s} dt / V_{CO_2}(t_I). \quad (3c)$$

195 By definition,  $F_f$ ,  $F_s$ , and  $F_l$  add up to one. Note that from these volumetric fractions,  
196 one can calculate the total volumes of the displaced brine leaking into other formations  
197 and stored in the seals and the storage formation, by multiplying these fractions by the  
198 volume of stored CO<sub>2</sub> at the final storage condition.

199 Note that  $V_{CO_2}$  is not the total volume of CO<sub>2</sub> at the injection condition; it is the total pore  
200 volume occupied by injected CO<sub>2</sub> under the final storage condition, depending on the  
201 density of CO<sub>2</sub>-rich phase. The necessary CO<sub>2</sub> storage capacity for a given site is often  
202 provided in total CO<sub>2</sub> mass,  $M_{CO_2}$ , instead of  $V_{CO_2}$ . Conversion of volume to mass is  
203 achieved through  $M_{CO_2} = \rho_{CO_2}(t_I)V_{CO_2}$ , in which the CO<sub>2</sub> density,  $\rho_{CO_2}$ , is evaluated at  
204 pressures and temperatures representing the final storage conditions. Because the  
205 pressure buildup caused by injection is not known beforehand for a given total CO<sub>2</sub> mass,  
206 the CO<sub>2</sub> density at storage conditions is either estimated a priori (in anticipation of an  
207 estimated pressure buildup) or determined in an iterative procedure, using the calculated  
208 average pressure to correct the density and vice versa.

### 209 **2.3. Application to Closed Systems**

210 In a closed system, the available volume for storage of CO<sub>2</sub> is provided only by the  
211 expansion of the pore volume and the increased brine density in response to pressure  
212 buildup in the storage formation. Equation (1) can then be simplified to the following  
213 linear expression:

$$214 \quad V_{CO_2}(t_I) = (\beta_p + \beta_w)\Delta p(t_I)V_f \quad (4)$$

215 This equation can be used, for example, to estimate the maximum storage capacity for a  
216 given sustainable pressure buildup,  $\Delta p_{\max}$ . Similarly, one can calculate the expected

217 average pressure buildup,  $\Delta p(t_I)$ , for a given total volume of stored CO<sub>2</sub> or a given CO<sub>2</sub>  
218 mass.

219 The storage efficiency factor of CO<sub>2</sub> storage in a closed system with average pressure  
220 buildup  $\Delta p(t_I)$  can be derived from a simplification of Equation (2)

$$221 \quad E = E_p(\Delta p(t_I)) + E_b(\Delta p(t_I)) = (\beta_p + \beta_w)\Delta p(t_I), \quad (5)$$

222 where  $E_p$  is the storage efficiency factor caused by pore compressibility, and  $E_b$  is the  
223 storage efficiency factor produced from brine compressibility. Inserting the sustainable  
224 pressure buildup,  $\Delta p_{\max}$ , into Equation (5) results in the maximum storage efficiency. For  
225 example, using  $\Delta p_{\max} = 6.0$  MPa, a pore compressibility of  $4.5 \times 10^{-10}$  Pa<sup>-1</sup> and a brine  
226 compressibility of  $3.5 \times 10^{-10}$  Pa<sup>-1</sup>, we arrive at  $E_p = 0.0027$  and  $E_b = 0.0021$ , and  $E =$   
227  $0.0048$ . In other words, less than half a percent of the total pore volume of a closed  
228 system would be available for the volumetric storage of CO<sub>2</sub> in a closed system during  
229 the injection period.

#### 230 **2.4. Application to Semi-Closed Systems**

231 Unlike the linear relationship of the total volumetric storage capacity and pressure  
232 buildup to pore and brine compressibilities for a closed system, such relationships for a  
233 semi-closed system are nonlinear and transient, with the pressure buildup in the storage  
234 formation affecting leakage rate through the seals, and vice versa. This makes solving of  
235 Equation (1) more complicated; however, a solution can be achieved through a simple  
236 numerical integration in time. For this purpose, the injection time period  $[0, t_I]$  can be  
237 discretized into a number ( $n$ ) of equally spaced time intervals of duration  $\Delta t$  to form a

238 time series:  $t_0, t_1, \dots, t_{i-1}, t_i, \dots, t_{n-1}, t_n$ , with  $t_0 = 0$  and  $t_n = t_f$ . Equation (1) converts  
 239 into its discrete form as follows:

$$240 \quad \Delta p(t_i) = \frac{V_{CO_2}(t_i) - \frac{2Ak_s \Delta t}{\mu_w B_s} \sum_{j=0}^{i-1} \Delta p(t_j)}{(\beta_p + \beta_w)V_f + 0.5(\beta_{ps} + \beta_w)V_s + \frac{Ak_s \Delta t}{\mu_w B_s}}, \quad i = [1, n]. \quad (6)$$

241 At each new time step, the pressure-buildup values at all previous time steps are known,  
 242 such that the summation term in Equation (6) (representing the cumulative brine leakage  
 243 from beginning of injection to the previous time step) can be executed. Equation (6)  
 244 eventually yields the pressure buildup at all time steps from the beginning to the end of  
 245 injection. Once Equation (6) has been solved, the storage efficiency factors in Equation  
 246 (2) or the volumetric fractions in Equation (3) can be derived using the known injection  
 247 and pressure history.

248 In the quick-assessment method, it is assumed that the semi-closed systems have a radial  
 249 impervious layer to bound the systems laterally. This method may not be applicable to  
 250 the systems bounded laterally by a permeable layer with a permeability value between  
 251 those of the storage formation and the overlying/underlying sealing units.

252 Note that continued CO<sub>2</sub> injection into a semi-closed system would eventually lead to a  
 253 steady-state condition at which the volumetric injection rate,  $Q_{CO_2}$  (as a function of the  
 254 steady-state storage condition), equals the rate of displaced brine leakage through the  
 255 seals, assuming that the geomechanical and hydraulic integrity of the storage unit and  
 256 seals is maintained. The pressure buildup,  $\Delta p_s$ , associated with this steady-state  
 257 condition can be calculated as follows:

258 
$$\Delta p_s = \frac{Q_{CO_2}}{2Ak_s / \mu_w B_s}, \quad Q_{CO_2} = \frac{G_{CO_2}}{\rho_{CO_2}(\Delta p_s)}, \quad (7)$$

259 where  $G_{CO_2}$  is the injection rate of CO<sub>2</sub> mass. If  $\Delta p_s$  is unrealistically high, i.e., higher  
260 than the sustainable pressure buildup, the storage capacity is pressure constrained and  
261 needs to be evaluated, using Equation (6). If, on the other hand,  $\Delta p_s$  is relatively small,  
262 brine leakage through the seals is sufficient to allow for significant CO<sub>2</sub> storage without  
263 pressurization concerns. In this case, the semi-closed system acts like an open storage  
264 formation, and its storage capacity is not pressure-constrained.

## 265 **2.5. Sustainable Pressure Buildup**

266 The CO<sub>2</sub> storage capacity of pressure-constrained systems depends on the *sustainable*  
267 *pressure buildup* that a given formation-seal system is expected to tolerate without  
268 geomechanical degradation (such as microfracturing and/or fault reactivation) of the  
269 sealing structures (USEPA, 1994; Neuzil, 2003; Rutqvist and Tsang, 2002; Rutqvist et  
270 al., 2007). Fluid pressure in the storage formation may also be constrained to limit the  
271 pressure driving forces into neighboring formations, or to account for potential concerns  
272 about seismicity. According to Rutqvist et al. (2007), the sustainable pressure buildup  
273 should be reviewed on a case-by-case basis, taking into account initial stress fields and  
274 geomechanical properties of the rock units at the selected sites.

275 Some guidance on the determination of a sustainable pressure buildup (for  
276 geomechanical damage) is provided by the current practice for underground injection  
277 control of liquid wastes. The regulatory standard states that maximum injection pressure  
278 should be less than the measured *fracture closure pressure*. Below the fracture closure  
279 pressure, any existing fractures cannot open and no new fractures can form, implying no

280 enhanced migration of waste fluids out of the injection intervals (USEPA, 1994). The  
281 regional guidance for implementation is that the maximum injection pressures can be  
282 determined either by a site-specific fracture closure pressure derived from direct or  
283 indirect testing, or by formation-specific default values for the fracture-closure pressure  
284 gradients. For example, a default value of 0.0129 MPa/m (130% of the hydrostatic  
285 pressure gradient) is given for the Mt. Simon Formation in Illinois, USA; 0.0181 MPa/m  
286 (181% of the hydrostatic pressure gradient) is reported for the Dundee Limestone in the  
287 Michigan Basin in USA. These fracture-closure pressure gradients correspond to  
288 sustainable fluid pressures of 15.5 and 21.7 MPa at 1,200 m depth, leading to sustainable  
289 pressure buildup of 3.5 and 9.7 MPa, respectively. In the following example applications,  
290 we chose a sustainable pressure buildup of 6.0 MPa, which corresponds to 50% of the  
291 initial hydrostatic pressure at the top (1,200 m) of the hypothetical storage formation.  
292 This value was used to demonstrate the quick-assessment method, and a site-specific  
293 value is needed when applied to a specific geologic site.

### 294 **3. Numerical Simulations and Results**

295 To validate the quick-assessment method discussed above, the “true” CO<sub>2</sub> storage  
296 capacity of closed or semi-closed formations was calculated through numerical  
297 simulation of the multiphase flow and multicomponent transport of CO<sub>2</sub> and brine in a  
298 hypothetical deep saline formation, using the TOUGH2/ECO2N simulator (Pruess, 2005;  
299 Pruess et al., 1999). The validity range of the quick-assessment method was demonstrated  
300 using different simulation runs, varying the radial extent to evaluate the effect of storage  
301 formation size, varying storage-formation properties to evaluate the uniformity of  
302 pressure buildup, and varying seal permeability to investigate the effect of brine leakage

303 into and through the seals and its impact on storage capacity. For each simulation run, we  
304 calculated the storage efficiency factor ( $E$ ) and the domain-averaged pressure buildup. If  
305 the simulated pressure buildup in the storage formation at the end of the injection period  
306 is less than the sustainable pressure buildup, the designated storage scenario is not  
307 pressure-constrained, and we refer to  $E$  as the *actual storage efficiency factor*. In contrast,  
308 in cases where the simulated pressure buildup exceeds the sustainable pressure buildup  
309 (which may occur before reaching the designated injection volume), the storage scenario  
310 is pressure-constrained. In such cases, we refer to  $E$  as the *maximum storage efficiency*  
311 *factor*, which corresponds to the sustainable pressure buildup.

### 312 **3.1. Model Setup**

313 A two-dimensional radially symmetric model domain was chosen to represent a deep  
314 saline aquifer. The storage formation, located at a depth of approximately 1,200 m below  
315 the ground surface, is 250 m thick and bounded at the top and bottom by sealing units  
316 (caprock and baserock) of 60 m thick each. The outer lateral boundary has a no-flow  
317 condition. In the base case, the model domain has a radial extent of 20 km, and the  
318 sealing units are assumed to be impervious. Carbon dioxide is injected in a zone of 125 m  
319 in thickness and 50 m in radial extent. Injection operates over 30 years at a rate of 120  
320 kg/s (i.e., annual rate of 3.8 million tonnes of CO<sub>2</sub>). The aquifer is initially fully brine-  
321 saturated, assuming a hydrostatic fluid pressure distribution. Isothermal conditions are  
322 modeled with a uniform temperature of 45°C. Table 1 lists the assigned values of  
323 hydrogeological properties typical of a homogeneous brine aquifer suitable for CO<sub>2</sub>  
324 storage. Note that the brine compressibility is intrinsically taken into account in  
325 TOUGH2/ECO2N in terms of density variation with fluid pressure.



326 The capacity of CO<sub>2</sub> storage in a closed or semi-closed system depends on the  
327 hydrogeological properties of the storage formation and the confining units (e.g.,  
328 permeability, porosity, and pore compressibility), and the total pore volume of the storage  
329 formation (e.g., thickness and radial extent). The sensitivity simulations conducted in this  
330 study are listed in Table 2. In each sensitivity case, only the property of interest was  
331 changed from the base-case value. The van Genuchten model was used to calculate the  
332 capillary pressure and the relative permeabilities for the two phase flow in all the  
333 simulation cases (van Genuchten, 1980). This model contains two fitting parameters  $\alpha$   
334 and  $m$ ; the van Genuchten  $\alpha$  parameter represents the inverse of the characteristic  
335 capillary pressure or roughly of the entry pressure for the nonwetting phase and the van  
336 Genuchten  $m$  parameter is a measure of the pore-size distribution. The  $\alpha$  and  $m$  values of  
337 the storage formation used in the simulations are  $5.1 \times 10^{-5} \text{ Pa}^{-1}$  and 0.46, respectively  
338 (Table 1). In Cases 10 through 13 with imperfect seals, the seal porosity and  $\alpha$   
339 parameter are 0.05 and  $5.1 \times 10^{-6} \text{ Pa}^{-1}$ , respectively. All other properties of the seals are  
340 identical to the storage formation. In the model, fixed hydrostatic pressure conditions are  
341 set at the top of the upper seal and the bottom of the lower seal.

### 342 **3.2. Results and Discussion**

343 Figures 2a and 2b show the spatial distributions of CO<sub>2</sub> saturation and pressure buildup  
344 (compared to the initial hydrostatic pressure) at the end of the 30-year injection period for  
345 the base case. The CO<sub>2</sub> plume is approximately 4 km wide and is concentrated at the top  
346 portion of the aquifer, a result of the buoyant CO<sub>2</sub> accumulating below the impervious  
347 caprock. As shown in Figure 2b, the region of elevated pressure is much larger than the  
348 CO<sub>2</sub> plume size. In fact, a substantial pressure increase is observed throughout the entire

349 20 km model domain, with the pressure buildup at the outer radial boundary at  
350 approximately 4.5 MPa. The pressure buildup near the injection zone is slightly higher  
351 than 6.0 MPa, thus exceeding the assumed sustainable threshold. Notice that the pressure-  
352 buildup contour lines away from the CO<sub>2</sub> plume region are mostly vertical, indicating  
353 horizontal brine displacement. Nonvertical contour lines can be seen in the CO<sub>2</sub> plume  
354 region, where the pressure conditions are affected by buoyancy and nonlinearity inherent  
355 in two-phase flow processes. We may conclude that this example features a pressure-  
356 constrained formation near or slightly beyond its capacity limits at the end of the  
357 designated injection time.

358 Radial pressure-buildup profiles at different times throughout the injection period are  
359 shown in Figure 3. At the very beginning of injection, the injected CO<sub>2</sub> displaces native  
360 brine in the area very close to the injection zone. The strong initial pressure buildup  
361 results from (1) the driving forces needed to move native brine away from the injection  
362 zone and (2) phase interference between aqueous and CO<sub>2</sub> phases in the region of two-  
363 phase flow (Pruess and Garcia, 2002). This pressure increase, referred to here as  
364 *injection-driven pressure buildup*, depends on the boundary condition (i.e., CO<sub>2</sub> injection  
365 rate in the injection zone, injection strategy), formation permeability, and two-phase flow  
366 conditions. The pressure pulse propagates away from the injection zone and reaches the  
367 outer radial boundary after approximately two years. After that, the pressure at the outer  
368 boundary starts to increase with injection time in an approximately linear manner; i.e., the  
369 entire model domain becomes overpressurized such that additional pore volume is made  
370 available to store the injected CO<sub>2</sub>. The pressure buildup related to the need for  
371 generating additional pore space is referred to as *storage-driven pressure buildup*, which

372 depends mainly on the pore compressibility of the formation (as well as on changes in  
373 brine density).

374 Cases 1 through 5 analyze different storage formation sizes, with radial extent ranging  
375 from 10 km to 100 km, including scenarios that range from clearly pressure-constrained  
376 to not pressure-constrained for the given injection volume. Figures 2c and 2d show the  
377 spatial distribution of CO<sub>2</sub> saturation and pressure buildup at the end of the 30-year  
378 injection period for the case of a domain of 100 km radial extent. Comparison of Figures  
379 2a and 2c indicates that the CO<sub>2</sub> plumes in both cases are generally similar in shape, with  
380 minor differences in the lateral extent of the plumes caused by differences in pressure  
381 buildup and thus CO<sub>2</sub> density. In contrast to the small difference in CO<sub>2</sub> plume extent, a  
382 significant difference in the pressure conditions is observed in Figures 2b and 2d. The  
383 larger model domain is not pressure-constrained, representing the pressure conditions of  
384 an open system. As a result, the maximum pressure increase near the injection zone,  
385 about half of which is observed in the 20 km case, mainly represents injection-driven  
386 pressure buildup. At a radial distance of 20 km, the pressure buildup is 0.8 MPa in the  
387 100 km case, significantly lower than the 4.5 MPa observed in the 20 km case. In the 10  
388 km case (not shown), the simulated total pressure buildup actually reaches an  
389 unrealistically high level at the end of 30-year injection, with maximum values above  
390 18.0 MPa. Injection would have to cease after approximately eight years to keep the  
391 actual pressure buildup smaller than the sustainable threshold of 6.0 MPa.

392 Figure 4 shows the sensitivity of local pressure buildup near the injection zone to the  
393 permeability and pore compressibility of the storage formation. For the case with higher  
394 permeability (one order of magnitude higher than the base case), the pressure buildup in

395 the formation is almost uniform over the entire domain, varying from 5.1 MPa close to  
396 the injection zone to 4.7 MPa at the outer boundary (Figure 4a). For the second case with  
397 a lower permeability (a factor of two lower than the base case), a strong local pressure  
398 buildup near the injection zone leads to fluid pressure buildup in excess of the assumed  
399 sustainable threshold of 6.0 MPa—see Figure 4b. As a result, the permeability of the  
400 storage formation influences both the uniformity of pressure buildup over the domain and  
401 the propagation velocity of the pressure pulse away from injection zone. This behavior  
402 can be explained easily using the two-dimensional radial flow equation (i.e., the diffusion  
403 equation for pressure propagation), and the diffusivity defined by  
404  $D_d = k/[\phi_f(\beta_w + \beta_p)\mu_w]$ , neglecting the two-phase flow within the CO<sub>2</sub> plume (de  
405 Marsily, 1986; Muggeridge et al., 2004). Pressure dissipates (diffuses) faster for higher  
406 permeability and/or lower compressibility.

407 As shown in Figures 4c and 4d, the domain-averaged pressure buildup at 30 years is 0.8  
408 and 9.0 MPa for the pore compressibility of  $4.5 \times 10^{-9}$  and  $4.5 \times 10^{-11}$  Pa<sup>-1</sup>, respectively.  
409 This indicates that for the case of lower pore compressibility, the system will be pressure-  
410 constrained, and the designated CO<sub>2</sub> mass cannot be safely injected into the closed  
411 system without geomechanical damage. The pore compressibility of the storage  
412 formation is a key input parameter in the quick-assessment method. Wide ranges of pore  
413 compressibility have been reported in the literature, depending on the subsurface  
414 materials (e.g., Fjaer et al., 1991; Domenico and Schwartz, 1998; Hart, 2000; Harris,  
415 2006).

416 Figure 5 shows horizontal profiles of pressure buildup at the top of the storage formation,  
417 as a function of seal permeability. The pressure buildup observed in the storage formation  
418 is very sensitive to increases in seal permeability. While the lowest seal permeability  
419 ( $10^{-20}$  m<sup>2</sup> or  $10^{-5}$  mD) shows a behavior similar to the closed system for the time scale  
420 relevant to estimating CO<sub>2</sub> storage capacity (i.e., the injection time period), we see a  
421 strong reduction of overall pressure buildup in all other cases, particularly those with  
422 permeabilities of  $10^{-18}$  and  $10^{-17}$  m<sup>2</sup>. In these cases, a significant fraction (e.g., 0.46 and  
423 0.93) of the displaced brine escapes from the storage formation into the seals, and  
424 through the seals into the overlying and underlying formations during the injection period  
425 of 30 years, thereby providing additional storage capacity for the injected CO<sub>2</sub> such that  
426 less pressure buildup occurs. We have calculated the cumulative fraction of displaced  
427 brine escaping from the storage formation relative to the total volume of stored CO<sub>2</sub> at in-  
428 situ conditions. With a seal permeability of  $10^{-20}$  m<sup>2</sup> ( $10^{-5}$  mD), this volume fraction is  
429 rather insignificant at 0.07, whereas with a seal permeability of  $10^{-17}$  m<sup>2</sup> ( $10^{-2}$  mD), this  
430 fraction increases to 0.93; i.e., the additional CO<sub>2</sub> storage capacity from brine leakage  
431 would amount to about 93% of the total injected CO<sub>2</sub> at 30 years. (In the latter case, the  
432 average Darcy's velocity in the seals is approximately 2.0 mm/year for the steady-state  
433 condition.) This effect can be very important for storage-capacity estimates in  
434 compartmentalized systems that have sealing units with small, but non-zero,  
435 permeability. Notice that the pressure profiles in Figure 5d remain relatively unchanged  
436 after a few years of injection, indicating that a quasi-steady state has been reached in  
437 which the volumetric rate of leakage of displaced brine is identical to the volumetric rate  
438 of injected CO<sub>2</sub> under final storage conditions.

439 In contrast to the significant leakage of displaced brine, negligible amounts of CO<sub>2</sub>  
440 escape from the storage formation into the seals. The cumulative fractions of CO<sub>2</sub> leaking  
441 into the caprock are 0.22, 0.35, 0.70, and 3.1% of the total injected CO<sub>2</sub> mass, for the seal  
442 permeability cases of 10<sup>-20</sup> (10<sup>-5</sup> mD) to 10<sup>-17</sup> m<sup>2</sup> (10<sup>-2</sup> mD) respectively. Most of this  
443 leakage is dissolved CO<sub>2</sub> that the quick-assessment method cannot account for, migrating  
444 with leaking brine from the storage formation into the seals. Carbon dioxide as the  
445 nonwetting-phase fluid needs to overcome a considerable capillary entry pressure before  
446 being able to migrate into the water-saturated pores of the sealing units. The observed  
447 migration of CO<sub>2</sub> within the seals is limited to the immediate vicinity of the storage  
448 formation; CO<sub>2</sub> is not able to escape into units overlying or underlying the seals. When a  
449 higher entry pressure is used (as represented by a smaller site-specific value of the van  
450 Genuchten  $\alpha$  parameter), the CO<sub>2</sub> phase leakage will be smaller.

451 The simulation results suggest that compartmentalized storage reservoirs with reasonably  
452 good, but imperfect, seals may allow for enough displaced brine leaking out of the  
453 formation to offset pressure-related storage limitations, while still having sufficient  
454 sealing capacity to trap supercritical CO<sub>2</sub>. Seal permeabilities can range over orders of  
455 magnitude, from 10<sup>-23</sup> to 10<sup>-16</sup> m<sup>2</sup> (Domenico and Schwartz, 1998; Hart et al., 2006;  
456 Hovorka et al., 2001; Neuzil, 1994). Relevant to geological CO<sub>2</sub> sequestration, the  
457 measured permeability of the sealing unit overlying the storage formation is  $1.0 \times 10^{-18}$   
458 m<sup>2</sup> (10<sup>-3</sup> mD) at the Frio test site (Doughty and Pruess, 2004; Hovorka et al., 2001), and  
459 0.75 to  $1.5 \times 10^{-18}$  m<sup>2</sup> at the Sleipner site (Chadwick et al., 2007).

#### 460 **4. Validity of the Quick-Assessment Method**

461 To validate the quick-assessment method, we derived quick estimates of domain-  
462 averaged pressure buildup and storage efficiency factors for the simulation scenarios  
463 discussed above, and compared those estimates with their corresponding “true” values  
464 obtained via detailed numerical simulations.

##### 465 **4.1. Comparison of Pressure-Buildup Estimates**

466 The first step in demonstrating the validity of the quick-assessment method is to compare  
467 the estimated domain-averaged pressure buildup against the numerical simulation results  
468 for both closed and semi-closed systems. Figure 6a shows domain-averaged pressure  
469 buildup, as a function of injection time, for closed systems of varying total pore volume  
470 (Cases 1 through 5 in Table 2). The quick-assessment estimates have been obtained using  
471 Equation (4), solving for pressure buildup  $\Delta p(t)$  at given times  $t$  during the injection  
472 period. The corresponding cumulative CO<sub>2</sub> volume  $V_{CO_2}(t)$  at each time step  $t$  is derived  
473 from the constant CO<sub>2</sub> injection rate of 120 kg/s used in the numerical simulation, and the  
474 CO<sub>2</sub> density under the storage condition. Conversion from CO<sub>2</sub> mass to CO<sub>2</sub> volume is  
475 conducted at each time step using the CO<sub>2</sub> density calculated at average pressure  
476 conditions. The agreement between the true numerical solutions and the quick estimates  
477 is excellent, considering that several simplifications and assumptions are involved in the  
478 quick-assessment method (e.g., uniform pressure buildup in domain, no dissolution,  
479 constant compressibility values). In Case 2, with 10 km radial extent, pressure builds up  
480 to values exceeding the sustainable pressure threshold soon after injection.

481 Figures 6b and 6c show domain-averaged pressure buildup for the closed-system cases  
482 with varying formation permeability (Cases 1, 6, and 7 in Table 2) and varying pore

483 compressibility (Cases 1, 8, and 9 in Table 2), for a radial extent of 20 km. The results of  
484 the quick-assessment method are independent of formation permeability, and only one  
485 profile obtained by the quick-assessment method is shown in Figure 6b. The agreement  
486 between simulated and estimated average pressure buildup is very good. While formation  
487 permeability defines the magnitude of local injection-driven pressure buildup (see Figure  
488 4), the average pressure change over the entire domain is hardly affected by permeability  
489 changes. Pore compressibility, in contrast, has a strong impact on the average pressure  
490 buildup in response to CO<sub>2</sub> injection (Figure 6c). In the case with the lowest pore  
491 compressibility, pressure buildup is so strong that the designated CO<sub>2</sub> volume cannot be  
492 safely stored. Since pore compressibility is a parameter explicitly accounted for in the  
493 quick-assessment method, the quick-assessment estimates provide an accurate  
494 representation of the detailed simulation results.

495 Figure 6d shows a similar comparison of domain-averaged pressure buildup for the semi-  
496 closed system with nonideal seals of different permeability (Cases 10 through 13). In  
497 these cases, the quick-assessment estimates are obtained using Equation (6). Overall, the  
498 agreement between estimated and numerical results is reasonably good, with a maximum  
499 discrepancy of less than 6%. While the quick-assessment method captures well the  
500 general transient, nonlinear trends in pressure buildup, it slightly underestimates the  
501 pressure buildup for the case with the lowest seal permeability (i.e., 10<sup>-20</sup> m<sup>2</sup> or 10<sup>-5</sup> mD)  
502 and slightly overestimates pressure buildup in the cases with relatively high seal  
503 permeability (e.g., 10<sup>-17</sup> m<sup>2</sup> or 10<sup>-2</sup> mD).

504 Both numerical and estimated results show clearly that the average pressure approaches  
505 an asymptotic maximum after a few years for the case with the relatively high seal  
506 permeability of 10<sup>-17</sup> m<sup>2</sup> (Figure 6d). This indicates a steady-state condition with equal  
507 volumetric rates of CO<sub>2</sub> entering and displaced brine leaving the storage formation. We



508 apply Equation (7) to estimate the average pressure buildup that would correspond to  
509 such a condition and arrive at values of 0.34, 3.23, and 27.02 MPa for the three cases  
510 with seal permeabilities of  $10^{-17}$ ,  $10^{-18}$ , and  $10^{-19}$  m<sup>2</sup> ( $10^{-2}$ ,  $10^{-3}$ ,  $10^{-4}$  mD), respectively. In  
511 the first case, the estimated value is identical to the final pressure buildup shown in  
512 Figure 6d. In the second case, a steady-state condition has not yet been established after  
513 30 years of injection, but would be reached if injection would continue for a few more  
514 years. The pressure value of 3.23 MPa associated with this steady-state condition is less  
515 than the sustainable pressure threshold, indicating that this scenario would not be  
516 pressure-constrained even if the injection period were much longer. In the third case,  
517 however, with a seal permeability of  $10^{-19}$  ( $10^{-4}$  mD) or less, a steady-state condition  
518 cannot be reached without geomechanical degradation.

519 In summary, the quick-assessment method provides reliable pressure estimates that can  
520 be compared with the sustainable pressure buildup to judge whether the designated  
521 volume of CO<sub>2</sub> can be safely stored in a storage formation, with or without vertical  
522 interlayer communication with other formations.

#### 523 **4.2. Comparison of Storage Efficiency Factors for Closed Systems**

524 We now compare the calculated and estimated (actual) storage efficiency factors of CO<sub>2</sub>  
525 storage in a closed system with different total pore volume (i.e., radial extents of 10, 20,  
526 30, 50, 100 km). The estimated values are obtained using Equation (5) and the pressure  
527 buildup calculated from Equation (4) for the same injection and storage-formation  
528 conditions as in the numerical simulations. We calculate the actual storage efficiency  
529 factor corresponding to the considered scenarios of injection and observed pressure  
530 buildup, regardless of whether this pressure buildup is higher than the sustainable

531 pressure buildup. Notice that the simulated storage efficiency factors include storage  
532 contributions from CO<sub>2</sub> in supercritical phase, as well as CO<sub>2</sub> dissolved in brine.

533 Table 3 shows the comparison of the actual storage efficiency factors for each case after  
534 30 years of injection, indicating reasonable agreement between estimated and calculated  
535 results. The quick-assessment estimates are slightly higher than those obtained through  
536 detailed numerical simulations. The significant decrease in the actual storage efficiency  
537 factor is observed with the increase in the radial extent, because of the decrease in the  
538 pressure buildup. In comparison, the maximum storage efficiency factor, calculated using  
539 the sustainable pressure buildup of 6.0 MPa and assigned brine and pore compressibilities  
540 would be  $E = 0.0048$ . The calculated actual storage efficiency factors can be evaluated  
541 against the maximum storage efficiency factor to check whether the designated CO<sub>2</sub>  
542 volume can be safely stored.

#### 543 **4.3. Comparison of Storage Contributions for Semi-Closed Systems**

544 In this validation exercise, we compare the three volumetric fractions for a semi-closed  
545 system obtained through the quick-assessment method (using Equations 3a through 3c)  
546 against those directly derived from the numerical simulations. Table 4 summarizes the  
547 results at the end of the 30-year injection period for the different seal permeability cases.  
548 Most of the storage capacity is provided by the storage formation when seal permeability  
549 is low (e.g., more than 90% for seal permeability of  $10^{-20}$  m<sup>2</sup> or  $10^{-5}$  mD). In contrast,  
550 most of the storage capacity is provided by brine escaping through the seals when seal  
551 permeability is comparably high (e.g., more than 90% for seal permeability of  $10^{-17}$  m<sup>2</sup> or  
552  $10^{-2}$  mD). In all cases, the match between the simulated and estimated fractions is  
553 reasonably good. The largest relative discrepancies occur with respect to the seal storage

554 of brine, because of the assumed linear pressure variation within the seals in the quick-  
555 assessment method.

#### 556 **4.4. Adequacy of Important Assumptions and Simplifications**

557 As shown in the above comparisons, the quick-assessment method provides reasonable  
558 estimates for the CO<sub>2</sub> storage capacity and pressure buildup in closed and semi-closed  
559 saline formations at various conditions. The accuracy of these estimates depends on the  
560 degree to which the process-related assumptions are satisfied in a real problem. One  
561 assumption is that the pressure buildup throughout the entire storage formation is  
562 uniform. This assumption works well as long as the average pressure is reasonably  
563 representative of the true pressure conditions (or, in other words, if the injection-driven  
564 pressure buildup is less important than the storage-driven pressure buildup). The detailed  
565 simulations in Section 3.2 feature one sensitivity case with small formation permeability  
566 of  $5 \times 10^{-14}$  m<sup>2</sup> (50 mD), where injection pressure alone exceeds the sustainable threshold.  
567 The quick-assessment method is not applicable in this case.

568 We generally recommend judging the quick-assessment results with care, knowing that  
569 average pressure predictions may underestimate the local conditions near the injection  
570 zone. On the other hand, the assumption of negligible CO<sub>2</sub> dissolution leads to an  
571 overestimation of pressure buildup and an underestimation of CO<sub>2</sub> storage capacity. The  
572 resultant approximation error depends on the CO<sub>2</sub> solubility in brine (which in turn varies  
573 with pressure, temperature, and salinity) and the fraction of CO<sub>2</sub> in contact with water.  
574 The detailed numerical simulations presented in this study suggest that the mass fraction  
575 of CO<sub>2</sub> dissolved in brine ranges from 0.02 to 0.03, and that the dissolved CO<sub>2</sub> accounts  
576 for approximately 7% of the total injected CO<sub>2</sub> mass at the end of 30-year injection.

577 Carbon dioxide density is calculated based on the estimated domain-averaged pressure  
578 buildup at storage conditions and the initial hydrostatic pressure. The density calculation  
579 captures transient pressure changes, but still introduces some inaccuracies because the  
580 domain-averaged pressure buildup may differ from actual pressure conditions within the  
581 CO<sub>2</sub> plume (which, of course, define CO<sub>2</sub> density). For native brine, the assumption of  
582 constant viscosity and compressibility leads to negligible errors over the pressure range  
583 relevant in this study.

## 584 **5. Summary and Conclusions**

585 We evaluated the CO<sub>2</sub> storage capacity in compartmentalized structures, where potential  
586 storage formations are bounded laterally and by overlying/underlying seals. If CO<sub>2</sub> is  
587 injected at an industrial scale into such closed systems (with impervious seals) or semi-  
588 closed systems (with non-ideal seals), pressure buildup can have a limiting effect on CO<sub>2</sub>  
589 storage capacity. We developed a simple quick-assessment method to assess the expected  
590 pressure buildup and CO<sub>2</sub> storage capacity in such potentially pressure-constrained  
591 systems. For validation of the method, we used “true” results from a numerical  
592 simulation model, which captures all relevant multiphase processes, determining the  
593 transient pressure buildup and CO<sub>2</sub> plume evolution in a hypothetical two-dimensional  
594 radial system.

595 The validity of the proposed method was demonstrated by the good agreement between  
596 the simple estimates and the numerical results regarding (1) the pressure buildup history  
597 over the injection period and (2) the storage efficiency factor calculated at the end of the  
598 injection period. We consider the new method useful for site selection and  
599 characterization, when storage capacity estimates may have to be compared over a large

600 number of sites. For a storage formation of relatively low permeability, the quick-  
601 assessment method may not be suitable because of low injectivity and high degree of  
602 non-uniformity of the pressure field, and detailed numerical simulations are required.

603 One interesting finding of this research is the importance of upper- and lower-seal  
604 permeability on pressure buildup in the storage formation. Closed systems with  
605 impermeable seals allow CO<sub>2</sub> storage only up to the point at which pressure in the storage  
606 formation approaches a sustainable threshold. This pressure constraint translates into  
607 small storage efficiency, on the order of 0.5% of the initial pore space for a typical pore  
608 compressibility value. However, only storage-formation-seal systems with very low seal  
609 permeabilities of 10<sup>-20</sup> m<sup>2</sup> or less exhibit such a closed-system behavior at the time scale  
610 of interest to capacity estimation; i.e., the leakage of native brine into and through the  
611 bounding seals is so small that the observed pressure buildup is similar to a closed  
612 system. With seal permeability varying from 10<sup>-19</sup> to 10<sup>-17</sup> m<sup>2</sup>, brine leakage into and  
613 through the seals had a moderate to strong effect in reducing or limiting the pressure  
614 buildup in the storage formation, thus allowing for considerably higher storage  
615 efficiency, while CO<sub>2</sub> was still safely trapped because of the combined capillary and  
616 permeability barriers. Our results indicate that a semi-closed system with seal  
617 permeability of 10<sup>-17</sup> m<sup>2</sup> is essentially an open system with respect to pressure buildup,  
618 because the rate of displaced brine leaking through the seals equals the rate of injected  
619 CO<sub>2</sub> at a later time of injection.

## 620 **Acknowledgments**

621 The authors wish to thank Curtis M. Oldenburg at Lawrence Berkeley National  
622 Laboratory (LBNL) for his careful internal review of the manuscript. Thanks are also due

623 to Dr. Stefan Bachu, the Associate Editor, and two anonymous reviewers for their  
624 constructive suggestions for improving the quality of the manuscript. This work was  
625 funded by the Assistant Secretary for Fossil Energy, Office of Sequestration, Hydrogen,  
626 and Clean Coal Fuels, National Energy Technology Laboratory, of the U.S. Department  
627 of Energy, and by Lawrence Berkeley National Laboratory under Contract No. DE-  
628 AC02-05CH11231.

## 629 **References**

- 630 Allis, R., Chidsey, T., Gwynn, W, Morgan, C., White, S., Adams, M., Moore, J., 2001.  
631 Natural CO<sub>2</sub> reservoirs on the Colorado Plateau and Southern Rocky Mountains:  
632 Candidates for CO<sub>2</sub> sequestration, in the Proceedings of First National Conference  
633 of Carbon Sequestration, National Energy Technology Laboratory, Washington  
634 DC, USA, May 15-17, 2001.
- 635 Bachu, S., 2002. Sequestration of CO<sub>2</sub> in geological media in response to climate change:  
636 road map for site selection using the transform of the geological space into the CO<sub>2</sub>  
637 phase space. *Energy Convers. Manage.* 43, 87-102.
- 638 Bachu, S., Adams, J.J., 2003. Sequestration of CO<sub>2</sub> in geological media in response to  
639 climate change: capacity of deep saline aquifers to sequester CO<sub>2</sub> in solution.  
640 *Energy Convers. Manage.* 44, 3151–3175.
- 641 Bachu, S., Gunter, W.D., Perkins, E.H., 1994. Aquifer disposal of CO<sub>2</sub>: Hydrodynamic  
642 and mineral trapping. *Energy Convers. Manage.* 35(4), 269–279.
- 643 Birkholzer, J.T., Zhou, Q., Rutqvist, J., Jordan, P., Zhang, K., Tsang, C.-F., 2007.  
644 Research Project on CO<sub>2</sub> Geological Storage and Groundwater Resources: Large-  
645 Scale Hydrogeological Evaluation and Impact on Groundwater Systems, Report  
646 LBNL-63544, Lawrence Berkeley National Laboratory, Berkeley, CA, USA.
- 647 Bradshaw, J., Bachu, S., Bonijoly, D., Burruss, R., Holloway, S., Christensen, N.P.,  
648 Mathiassen, O.M., 2007. CO<sub>2</sub> storage capacity estimation: issues and development  
649 of standards. *International J. Greenhouse Gas Control* 1(1), 62-68.
- 650 de Marsily, G., 1986. *Quantitative Hydrogeology*, Academic Press, Inc, San Diego.

651 Domenico, P.A., Schwartz, F.W., 1998. Physical and Chemical Hydrogeology, 2nd ed.  
652 John Wiley & Sons, Inc., New York.

653 Doughty, C., Pruess, K., 2004. Modeling supercritical carbon dioxide injection in  
654 heterogeneous porous media. *Vadose Zone J.* 3, 837–847.

655 Fjaer, E., Holt, R.M., Horsrud, P., Raaen, A.M., 1991. Petroleum Related Rock  
656 Mechanics. Elsevier, Amsterdam.

657 Harris, J.M., 2006. Seismic Monitoring of CO<sub>2</sub> Sequestration, GCEP Technical Report,  
658 Stanford University, Palo Alto, CA, USA.

659 Hart, D.J., 2000. Laboratory Measurements of Poroelastic Constants and Flow  
660 Parameters and Some Associated Phenomena. Ph.D. Thesis, University of  
661 Wisconsin-Madison, Madison, WI, USA.

662 Hart, D.J., Bradbury, K.R., Feinstein, D.T., 2006. The vertical hydraulic conductivity of  
663 an aquitard at two spatial scales. *Ground Water* 44(2), 201-211.

664 Holloway, S., Heederik, J.P., van der Meer, L.G.H., Czernichowski-Lauriol, I., Harrison,  
665 R., Lindeberg, E., Summerfield, I.R., Rochelle, C., Schwarzkopf, T., Kaarstad, O.,  
666 Berger, B., 1996. The Underground Disposal of Carbon Dioxide: Summary Report,  
667 JOULE II Project No. CT92-0031, British Geological Survey, Keyworth, UK.

668 Hovorka, S.D., Doughty, C., Knox, P.R., Green, C.T., Pruess, K., Benson, S.M., 2001.  
669 Evaluation of brine-bearing sands of the Frio formation, upper Texas gulf coast for  
670 geological sequestration of CO<sub>2</sub>, in: First National Conference on Carbon  
671 Sequestration, National Energy Technology Laboratory, Pittsburgh, PA, USA, 14–  
672 17 May, 2001.

673 IPCC (Intergovernmental Panel on Climate Change), 2005. IPCC Special Report on  
674 Carbon Dioxide Capture and Storage. Cambridge University Press, New York.

675 Koide, H., Tazaki, Y., Noguchi, Y., Nakayama, S., Iijima, M., Ito, K., Shindo, Y., 1992.  
676 Subterranean containment and long-term storage of carbon dioxide in unused  
677 aquifers and in depleted natural gas reservoirs. *Energy Convers. Manage.* 33(5–8),  
678 619–626.

679 Muggeridge, A., Abacioglu, Y., England, W., Smalley, C., 2004. Dissipation of  
680 anomalous pressures in the subsurface. *J. Geophys. Res.* 109, B11104,  
681 doi:10.1029/2003JB002922.

682 Neuzil, C.E., 1994. How permeable are clays and shales? *Water Resour. Res.* 30(2), 145–  
683 150.

684 Neuzil, C.E., 1995. Abnormal pressures as hydrodynamic phenomena. *Am. J. Science*  
685 295, 742-786.

686 Neuzil, C.E., 2003. Hydromechanical coupling in geologic processes. *Hydrogeol. J.* 11,  
687 41–83, DOI:10.1007/s10040-002-0230-8.

688 Nicot, J.-P., 2008. Evaluation of large-scale CO<sub>2</sub> storage on fresh-water sections of  
689 aquifers: an example from the Texas Gulf Coast Basin. *International J. Greenhouse*  
690 *Gas Control* (in revision).

691 Pearce, J.M., Holloway, S., Wacker, H., Nelis, M.K., Rochelle, C., Bateman, K., 1996.  
692 Natural occurrence as analogues for the geological disposal of carbon dioxide.  
693 *Energy Convers. Manage.* 37(6-8), 1123-1128.

694 Polak, S., Lundin, E., Bøe, R., Lindeberg, E.G.B., Olesen, O., Zweigel, P. 2004. Storage  
695 Potential for CO<sub>2</sub> in the Beitstadfjord Basin, Mid-Norway, Report SINTEF No.  
696 54.5272.00/01/04 and NGU No. 2004.036. 51p, Geological Survey of Norway,  
697 Trondheim, Norway.

698 Pruess, K., 2005. ECO2N: A TOUGH2 Fluid Property Module for Mixtures of Water,  
699 NaCl, and CO<sub>2</sub>, Report LBNL-57952, Lawrence Berkeley National Laboratory,  
700 Berkeley, CA, USA.

701 Pruess, K., Garcia, J., 2002. Multiphase flow dynamics during CO<sub>2</sub> disposal into saline  
702 aquifers. *Environ. Geol.* 42, 282–295.

703 Pruess, K., Oldenburg, C.M., Moridis, G., 1999. TOUGH2 User's Guide, version 2.0.  
704 Report LBNL-43134, Lawrence Berkeley National Laboratory, Berkeley, CA,  
705 USA.

706 Pruess K., García, J., Kavscek, T., Oldenburg, C. M., Rutqvist, J., Steefel, C., and Xu, T.,  
707 2004. Code intercomparison builds confidence in numerical simulation models for  
708 geologic disposal of CO<sub>2</sub>. *Energy*, 29(9-10), 1431-1444.



709 Puckette, J., Al-Shaieb, Z., 2003. Naturally underpressured reservoirs: applying the  
710 compartment concept to the safe disposal of liquid waste. In: search and discovery  
711 article 40071, online adaptation of presentation at American Association of  
712 Petroleum Geologists, southwest section meeting, Fort Worth, TX, USA, March,  
713 2003 ([www.southwestsection.org](http://www.southwestsection.org)).

714 Rutqvist, J., Tsang, C.F., 2002. A study of caprock hydromechanical changes associated  
715 with CO<sub>2</sub>-injection into a brine formation. *Environ. Geol.* 42, 296-305.

716 Rutqvist, J., Birkholzer, J.T., Cappa, F., Tsang, C.F., 2007. Estimating maximum  
717 sustainable injection pressure during geological sequestration of CO<sub>2</sub> using coupled  
718 fluid flow and geomechanical fault-slip analysis. *Energy Convers. Manage.* 48,  
719 1798-1807.

720 Shafeen, A., Croiset, E., Douglas, P.L., Chatzis, I., 2004. CO<sub>2</sub> sequestration in Ontario,  
721 Canada, Part I: storage evaluation of potential reservoirs. *Energy Convers. Manage.*  
722 45, 2645–2659.

723 Stevens, S.H., Pearce, J.M., Rigg, A.A.J., 2001. Natural analog for geologic storage of  
724 CO<sub>2</sub>: An integrated global research program, in the Proceedings of First National  
725 Conference of Carbon Sequestration, National Energy Technology Laboratory,  
726 Washington D.C., USA, May 15-17, 2001.

727 USDOE (U.S. Department of Energy), 2007. Methodology for development of carbon  
728 sequestration capacity estimates, Appendix A in Carbon Sequestration Atlas of the  
729 United States and Canada, National Energy Technology Laboratory, Pittsburgh,  
730 PA, USA.

731 USEPA (U.S. Environmental Protection Agency), 1994. Determination of Maximum  
732 Injection Pressure for Class I Wells, United States Environmental Protection  
733 Agency Region 5—Underground Injection Control Section Regional Guidance #7.  
734 EPA, Washington DC, USA.

735 Van der Meer, L.G.H., 1992. Investigations regarding the storage of carbon dioxide in  
736 aquifers in the Netherlands. *Energy Convers. Manage.* 33 (5–8), 611–618.

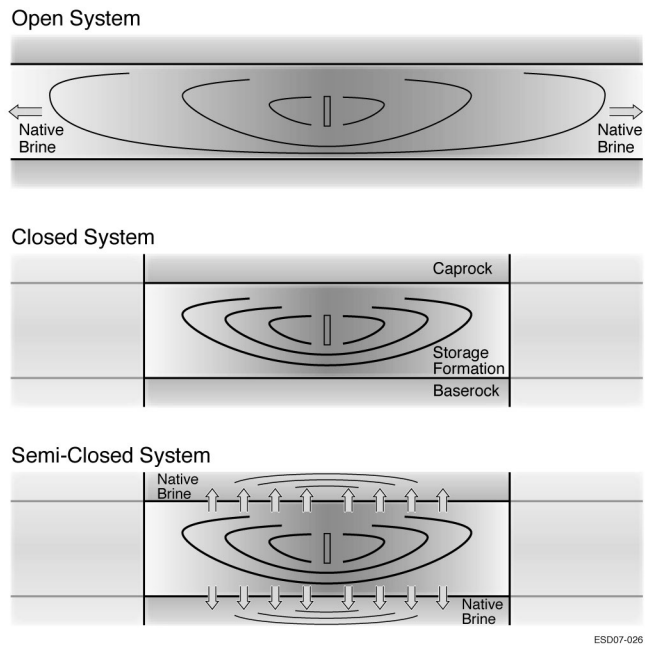
737 Van der Meer, L.G.H., 1995. The CO<sub>2</sub> storage efficiency of aquifers. *Energy Convers.*  
738 *Manage.* 36(6–9), 513–518.

739 Van Genuchten, M.T., 1980. A closed form equation for predicting the hydraulic  
740 conductivity of unsaturated soils. Soil Sci. Soc. Am. J. 44, 892–898.

- 741 Figure 1. Schematic showing open systems versus closed or semi-closed systems (not to  
742 scale)
- 743 Figure 2. Spatial distributions, simulated at 30 years of CO<sub>2</sub> injection, of (a) CO<sub>2</sub>  
744 saturation and (b) pressure buildup for the base case with the closed domain of  
745 a 20 km radial extent, and (c) CO<sub>2</sub> saturation and (d) pressure buildup for the  
746 case of a closed domain of 100 km radial extent. Figures 2a and 2c show  
747 close-ups of the CO<sub>2</sub> plume region with two-phase flow of CO<sub>2</sub> and brine
- 748 Figure 3. Pressure-buildup profiles along the aquifer top at different injection times.  
749 Filled squares indicate the CO<sub>2</sub> plume extent to show the radial extent of the  
750 evolving two-phase flow region
- 751 Figure 4. Horizontal profiles of pressure buildup at different times of CO<sub>2</sub> injection for  
752 formation permeability of (a)  $10^{-12}$  and (b)  $5 \times 10^{-14}$  m<sup>2</sup>, and pore  
753 compressibility of (c)  $4.5 \times 10^{-9}$  and (d)  $4.5 \times 10^{-11}$  Pa<sup>-1</sup>. All other parameters  
754 are kept the same as the base case. See comparison with Figure 3
- 755 Figure 5. Horizontal profiles of pressure buildup along the aquifer top at different times  
756 of CO<sub>2</sub> injection for seal permeability of (a)  $10^{-20}$ , (b)  $10^{-19}$ , (c)  $10^{-18}$ , and (d)  
757  $10^{-17}$  m<sup>2</sup>. See comparison with Figure 3
- 758 Figure 6. Comparison of the transient profiles of domain-averaged pressure buildup  
759 obtained through numerical simulations and through the quick-assessment  
760 method for (a) a closed system with varying radial extents  $R$ , (b) a closed  
761 system with radial extent  $R = 20$  km and varying formation permeability, (c) a  
762 closed system with radial extent  $R = 20$  km and varying pore compressibility,  
763 and (d) a semi-closed system with radial extent  $R = 20$  km and seals of  
764 varying permeability ( $k_s$ )

- 765 Table 1. Hydrogeologic properties for the storage formation and CO<sub>2</sub> injection rate used  
766 in the base-case simulations
- 767 Table 2. Numerical simulation runs for different radial extents of storage formation, and  
768 different values of permeability and pore compressibility of the storage  
769 formation, as well as permeability of the seals
- 770 Table 3. Comparison of the actual storage efficiency factors for CO<sub>2</sub> storage in closed  
771 systems, obtained through numerical simulation results and the quick-  
772 assessment method in Equation (5), at 30 years of injection
- 773 Table 4. Comparison between simulated and estimated volumetric fractions of  
774 displaced brine stored in the storage formation, in the seals, and in the  
775 overlying and underlying formations, relative to the total pore volume  
776 occupied by CO<sub>2</sub> at the end of the 30-year injection period, for different seal  
777 permeability values

778

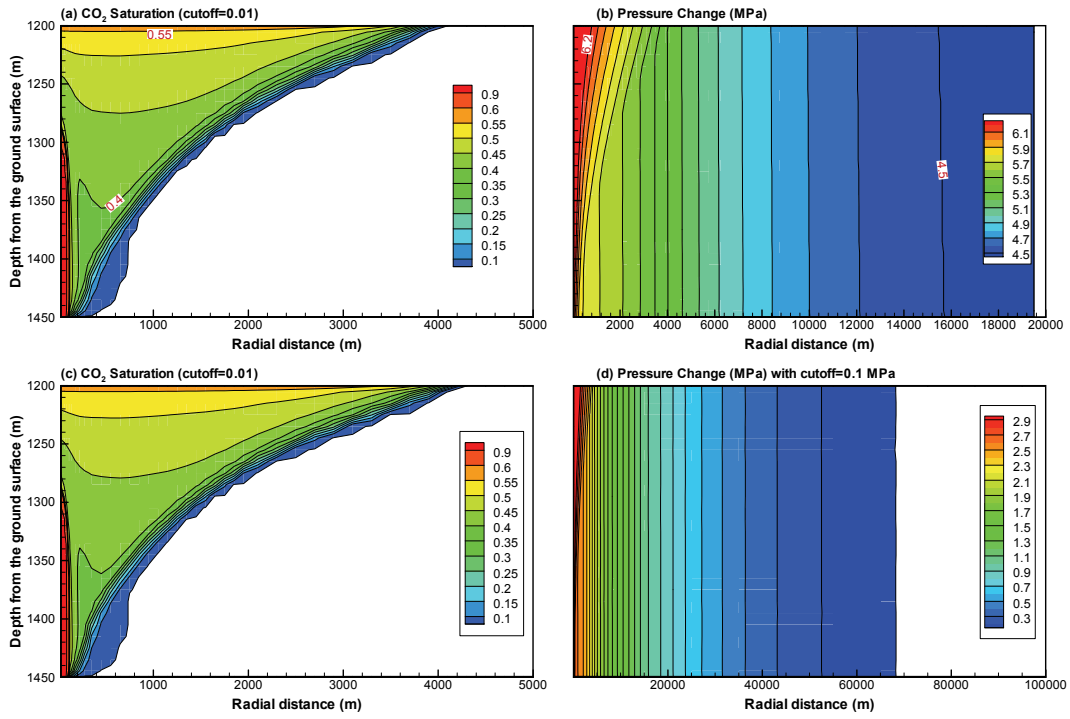


779

780 Figure 1.

ESD07-026

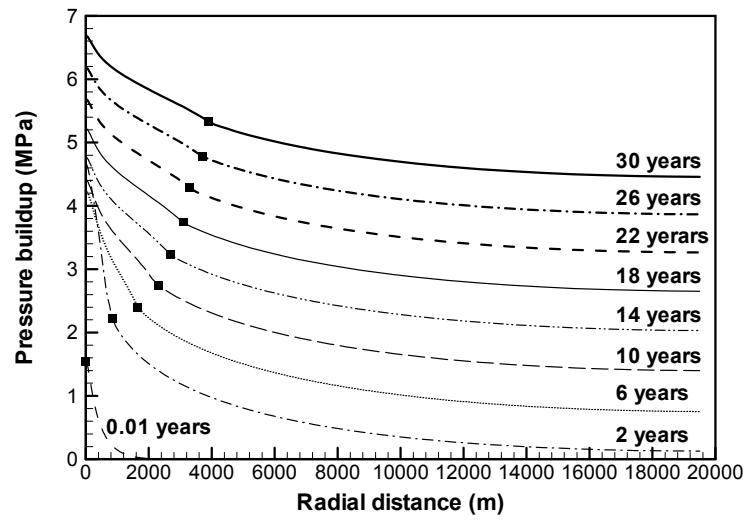
781  
782



783  
784

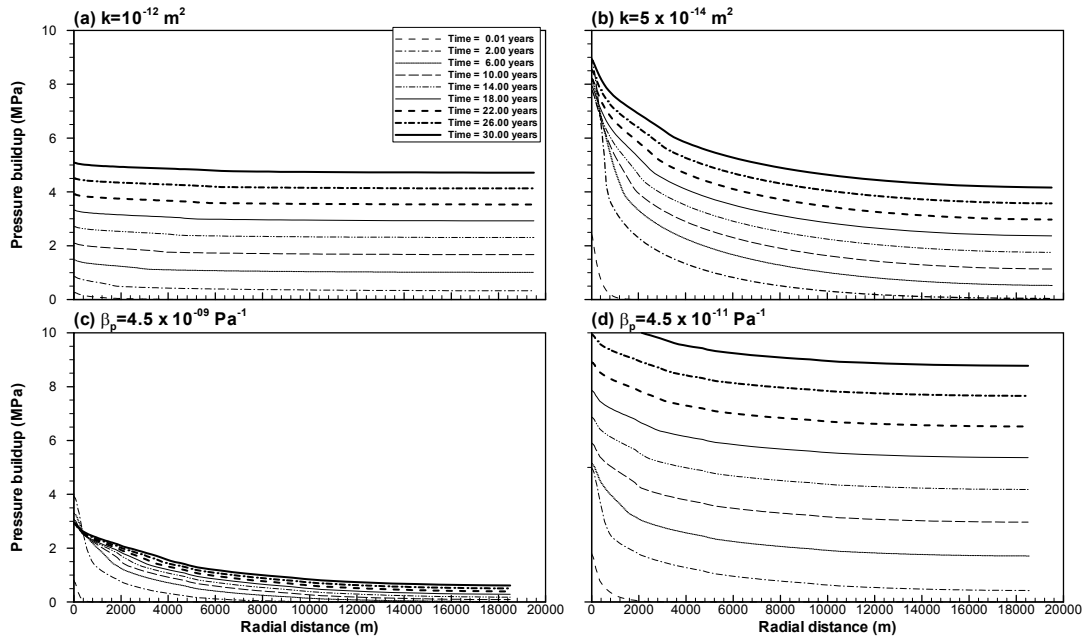
Figure 2.

785



786

787 Figure 3.

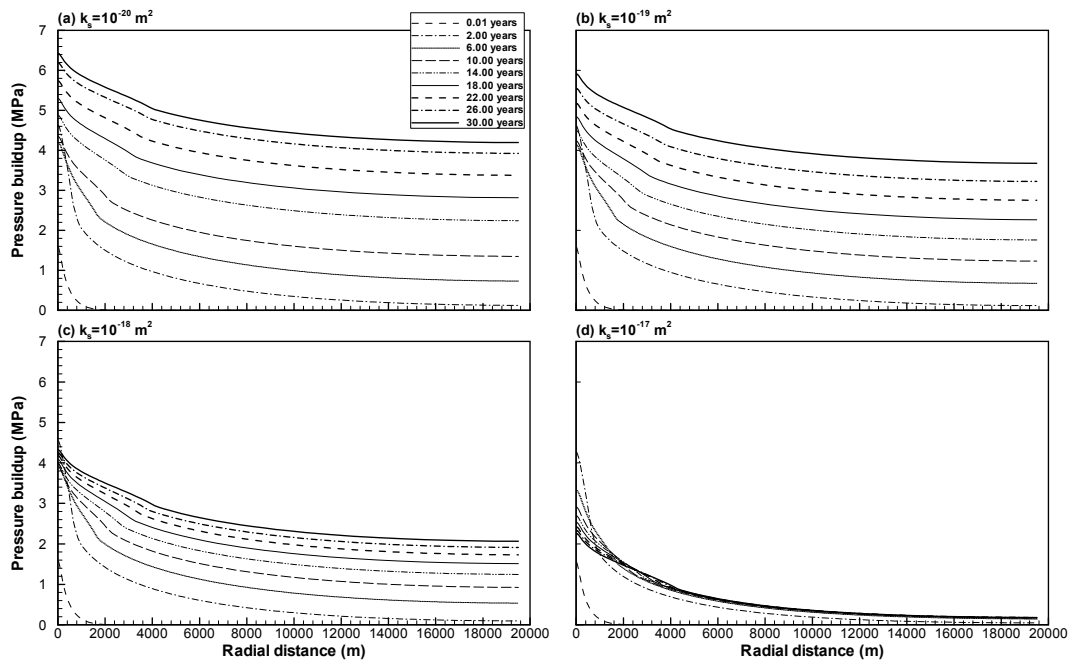


789

790

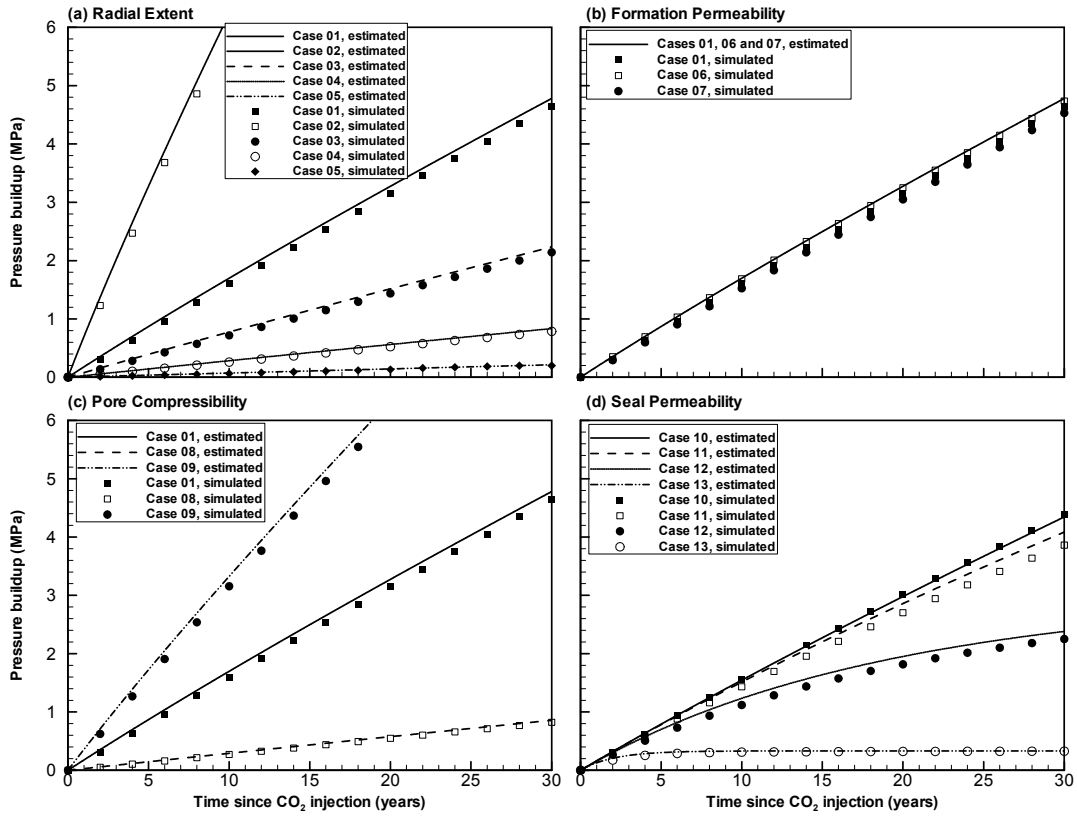
791 Figure 4.





793

794 Figure 5.



795

796 Figure 6.

797 Table 1.

<b>Properties</b>	<b>Values</b>
Horizontal permeability (m <sup>2</sup> )	10 <sup>-13</sup>
Vertical permeability (m <sup>2</sup> )	10 <sup>-13</sup>
Pore Compressibility (Pa <sup>-1</sup> )	4.5 × 10 <sup>-10</sup>
Porosity	0.12
van Genuchten (1980) <i>m</i>	0.46
van Genuchten $\alpha$ (Pa <sup>-1</sup> )	5.1 × 10 <sup>-5</sup>
Residual CO <sub>2</sub> saturation	0.05
Residual water saturation	0.30
CO <sub>2</sub> injection rate (kg/s)	120

798

799 Table 2.

	Case No	Radial Extent (km)	Formation Permeability (m <sup>2</sup> )	Formation Compressibility (Pa <sup>-1</sup> )	Seal Permeability (m <sup>2</sup> )
Base Case	Case 1	20	$1.0 \times 10^{-13}$	$4.5 \times 10^{-10}$	0
Storage Formation Volume	Case 2	10	$1.0 \times 10^{-13}$	$4.5 \times 10^{-10}$	0
	Case 3	30	$1.0 \times 10^{-13}$	$4.5 \times 10^{-10}$	0
	Case 4	50	$1.0 \times 10^{-13}$	$4.5 \times 10^{-10}$	0
	Case 5	100	$1.0 \times 10^{-13}$	$4.5 \times 10^{-10}$	0
Formation Permeability	Case 6	20	$1.0 \times 10^{-12}$	$4.5 \times 10^{-10}$	0
	Case 7	20	$5.0 \times 10^{-14}$	$4.5 \times 10^{-10}$	0
Formation Compressibility	Case 8	20	$1.0 \times 10^{-13}$	$4.5 \times 10^{-09}$	0
	Case 9	20	$1.0 \times 10^{-13}$	$4.5 \times 10^{-11}$	0
Seal Permeability	Case 10	20	$1.0 \times 10^{-13}$	$4.5 \times 10^{-10}$	$1.0 \times 10^{-20}$
	Case 11	20	$1.0 \times 10^{-13}$	$4.5 \times 10^{-10}$	$1.0 \times 10^{-19}$
	Case 12	20	$1.0 \times 10^{-13}$	$4.5 \times 10^{-10}$	$1.0 \times 10^{-18}$
	Case 13	20	$1.0 \times 10^{-13}$	$4.5 \times 10^{-10}$	$1.0 \times 10^{-17}$

800

801 Table 3.

		Simulation-Based Results			Quick-Assessment Estimates
Domain Radius (km)	Initial Pore Volume ( $10^9 \text{ m}^3$ )	Total Stored $\text{CO}_2$ Volume <sup>a</sup> ( $10^9 \text{ m}^3$ )	Average Pressure Buildup $\Delta p$ (MPa)	Actual Storage Efficiency Factor	Actual Storage Efficiency Factor
100	942.5	0.139	0.2	0.00015	0.00017
50	235.6	0.138	0.79	0.00059	0.00066
30	84.8	0.136	2.14	0.0016	0.0018
20	37.7	0.131	4.64	0.0035	0.0039
10	9.4	0.117	16.60 <sup>b</sup>	0.0124	0.014 <sup>b</sup>

802  
803

<sup>a</sup> Injected mass is identical for all domains. Stored volumes differ slightly because of different pressure/density conditions.

804  
805

<sup>b</sup> Average pressure buildup is higher than sustainable threshold. The calculated actual storage efficiency is therefore not feasible.

806

807

808 Table 4.

Seals Permeability	Simulation Results			Estimation by Equation (3)		
	Storage Formation	Seals	Other Formations	Storage Formation	Seals	Other Formations
$10^{-17} \text{ m}^2$	0.071	0.011	0.918	0.069	0.007	0.925
$10^{-18} \text{ m}^2$	0.470	0.104	0.426	0.500	0.050	0.450
$10^{-19} \text{ m}^2$	0.824	0.150	0.026	0.850	0.085	0.065
$10^{-20} \text{ m}^2$	0.931	0.059	0.010	0.903	0.090	0.007

809